



Summer school internship 2016

**Study of the impact of TS collimator misalignments  
on physics parameters of the Mu2e experiment**

Supervisor: Costas Vellidis

Work done by:  
Elisabetta Spadaro Norella

September 23, 2016

# Contents

- 1 Introduction** **3**
- 1.1 Mu2e experiment . . . . . 3
- 1.2 Backgrounds . . . . . 4
- 1.3 Mu2e design . . . . . 6
  - 1.3.1 Mu2e coordinate system . . . . . 7
- 1.4 Misalignment of the Transport Solenoid . . . . . 8
  - 1.4.1 Previous study . . . . . 8
  - 1.4.2 Purpose of my work . . . . . 8
  
- 2 Muons and pions stopping rates** **10**
- 2.1 Stopped particle simulation . . . . . 10
- 2.2 Results . . . . . 10
  
- 3 Beam electrons background** **14**
- 3.1 Simulation . . . . . 14
- 3.2 Results . . . . . 16
  
- 4 Beta source test** **18**
- 4.1 Simulations . . . . . 19
- 4.2 Results . . . . . 19
  
- 5 Conclusions** **24**

# Chapter 1

## Introduction

### 1.1 Mu2e experiment

The Mu2e experiment at Fermilab proposes to measure the ratio of the rate of the neutrinoless coherent conversion of muons into electrons in the field of a nucleus, relative to the rate of ordinary muon capture on the nucleus:

$$R_{\mu e} = \frac{\mu + A(Z, N) \rightarrow e + A(Z, N)}{\mu + A(Z, N) \rightarrow \mu + A(Z + 1, N)} \quad (1.1)$$

This quantity will be measured by the formation of  $10^{18}$  muonic Al atoms. Depending on the momentum and on the impact parameter of the incident muons with respect to the nucleus, the muon has a probability to be captured in different atomic shells. When muons are captured in higher shells, the muonic atom is in an excited state whose life time is  $< 1$  ps, i.e. much shorter than the life time of the ground state (864 ns). Muons then cascade to lower shells emitting X-rays. By using the ratio of Equation 1.1, common experimental and theoretical uncertainties in the numerator and denominator cancel out.

When the captured muon is in a 1s state, the muon and Al nucleus wave functions overlap, so that the muonic atoms are unstable and decay via three possible processes:

1. Nuclear capture ( 61%):  $\mu^- + {}_{13}^{27}Al \rightarrow \nu_\mu + {}_{12}^{27*}Mg$  ;
2. Muon decay in orbit ( 39%):  $\mu^- + {}_{13}^{27}Al \rightarrow e^- + \bar{\nu}_e + \nu_\mu + {}_{13}^{27}Al$ ;
3. Muon to electron conversion (  $< 10^{-12}$  ):  $\mu^- + {}_{13}^{27}Al \rightarrow e^- + {}_{13}^{27}Al$ .

The conversion process is the signal of the experiment, with a distinct signature of a single electron carrying an energy of  $E_e = -(m_\mu c^2 + E_{bind} + E_{recoil}) = 104.96 MeV$  , where  $E_{bind}$  is the binding energy of the muon with the Al nucleus and  $E_{recoil}$  is the kinetic energy of the recoiling Al nucleus. Muon decay in orbit (DIO) is the dominant background of the experiment, producing electrons of energy up to 104.96 MeV. Nuclear capture serves as a normalization (or "effective luminosity") factor for the signal, since it can be both calculated using the amplitude of muon capture in the electromagnetic field of an Al nucleus and measured by detecting the photons coming from cascade de-excitations of the excited daughter nuclei  $Mg^*$ . Mu2e intends to probe four orders of magnitude beyond the current best experimental limit, measuring  $R_{\mu e}$  with a single-event sensitivity of  $2.87 \cdot 10^{-17}$  . The conversion process is an example of charged lepton flavor violation (CLFV), a process that has never been observed experimentally. Observation of this process would provide unambiguous evidence for physics beyond the Standard Model (SM) and can help to illuminate discoveries made at the LHC or point to new physics beyond the reach of the LHC.

## 1.2 Backgrounds

At the proposed Mu2e sensitivity there are a number of processes that can mimic a  $\mu^- + N \rightarrow e^- + N$  signal. Controlling these potential backgrounds drives the overall design of Mu2e. These backgrounds result principally from five sources:

1. intrinsic processes that scale with beam intensity; these include muon decay-in-orbit (DIO) and radiative muon capture (RMC);
2. processes that are delayed because of particles that spiral slowly down the muon beam line, such as antiprotons;
3. prompt processes where the detected electron is nearly coincident in time with the arrival of a beam particle at the muon stopping target (e.g. radiative pion capture, RPC);
4. electrons or muons that are initiated by cosmic rays;
5. events that result from reconstruction errors induced by additional activity in the detector from conventional processes.

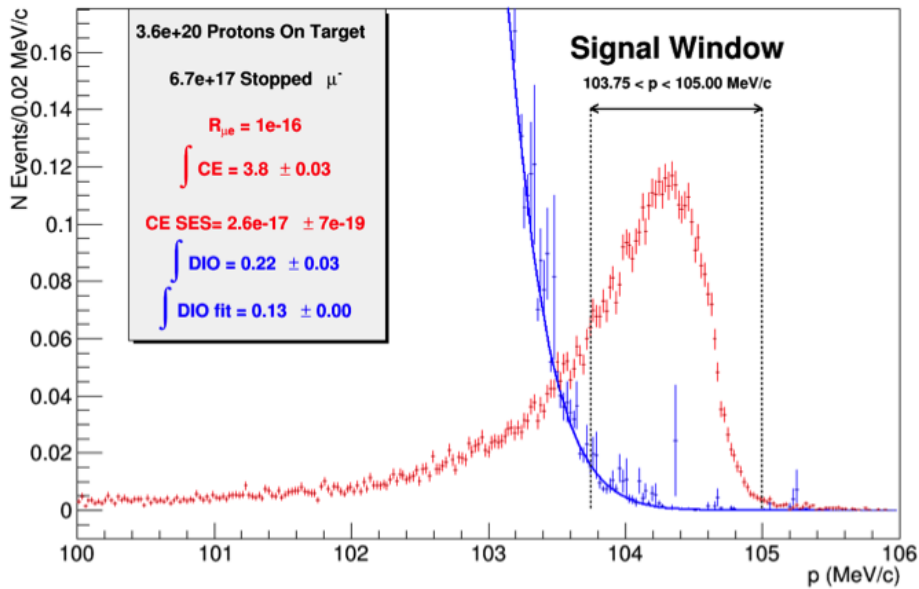


**Figure 1.1:** The simulated-reconstructed momentum spectrum for DIO events (blue) and conversion electron (CE) events surviving the track selection criteria and assuming  $R_{\mu e} = 10^{-16}$ . The distributions are each normalized to the total number of muon stops expected for  $3.6 \times 10^{20}$  protons on target.

DIO produces electrons with a continuous energy spectrum, as shown in blue in Figure 1.1; the shape is a distorted Michel spectrum with a long tail, due to radiative corrections in which the outgoing electron coherently exchanges photons with the nucleus or emits real photons which escape detection. In one extreme configuration, both neutrinos are at rest and the electron recoils against the intact Al nucleus. This is the configuration in which the electron has the maximum energy in the lab frame, about 105 MeV for muonic Al. This energy is equal to the muon mass, less a small correction for the K-shell binding energy and an even smaller correction for nuclear recoil. The  $\mu$  to  $e$  conversion process produces a mono-energetic electron with an energy equal to that of the endpoint of the continuous spectrum from DIO. An irreducible background comes from electrons in the high energy tail of the DIO spectrum that are mis-measured with a momentum in the signal region. Because of the rapid decrease in the DIO rate as the electron energy approaches the end point (approximately as  $(E_{\text{endpoint}} - E_e)^5$ ), the background

can be suppressed through adequate resolution on the electron momentum. To reduce the DIO background, the central part of the energy resolution function must be narrow and high energy tails must be suppressed. This depends on the intrinsic resolution of the tracker detector as well as on the amount of material traversed by conversion electrons (CE).

Muons can also undergo radiative muonic capture (RMC) on the nucleus ( $\mu^- + Al \rightarrow \nu_\mu + Mg + \gamma$ ). The photon can be emitted internally or externally and convert to electron-positron pair in the stopping target or other surrounding material, producing an electron near the conversion electron energy.

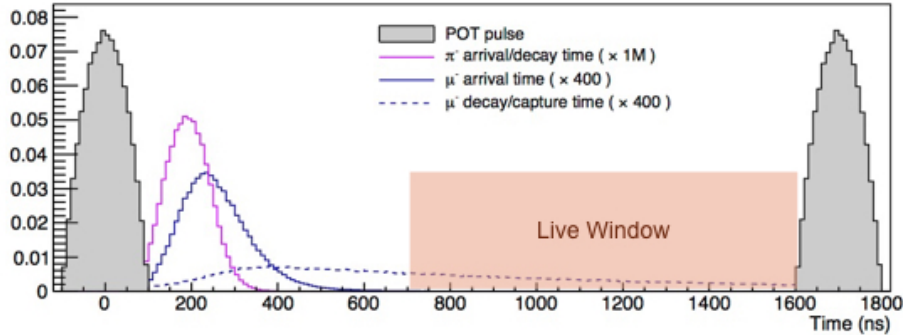


**Figure 1.2:** The Mu2e spill cycle for the proton beam and the delayed search window that allows for the effective elimination of prompt backgrounds when the number of protons between the pulses is suppressed to the required level. The width of proton of target (POT) pulse is of 250 ns, while the prompt flash lasts 700 ns. The start time and duration of the search window (995 ns) shown in the figure is illustrative. The exact delay and duration are optimized to keep pion-capture backgrounds at a low level.

The  $\mu^-$  beam that reaches the stopping target is contaminated by many  $e^-$  and some  $\pi^-$ , both of which can produce false signals when they interact with the stopping targets. Pions can produce background when they are absorbed in the stopping target or surrounding material and produce a high energy photon through radiative pion capture (RPC):

$$\pi^- + N \rightarrow \gamma + N^*; \quad (1.2)$$

The outgoing photon can again convert to electron-positron pair, producing an electron that can mimic the signal. To defeat RPC and other prompt backgrounds, the experiment exploits the lifetime of muonic Al, about 864 ns: as illustrated in Figure 1.2, Mu2e waits for 700 ns following the arrival of the proton bunch at the production target and then begins counting electrons that are emitted from the foils of the stopping target. By this time, all of the beam from the production target has passed through the stopping target and the prompt backgrounds have died away. After a total of 1695 ns the cycle is repeated.

It is also critical that few protons arrive at the production target between the bunches. If protons arrive out of time, they can produce  $e^-$  and  $\pi^-$  that arrive at the stopping target within the live gate. To reduce this background Mu2e requires an extinction factor of  $10^{-10}$ ; that is, for every  $10^{10}$  protons arriving at the production target within the bunch, there should be no more than 1 proton arriving between bunches.

### 1.3 Mu2e design

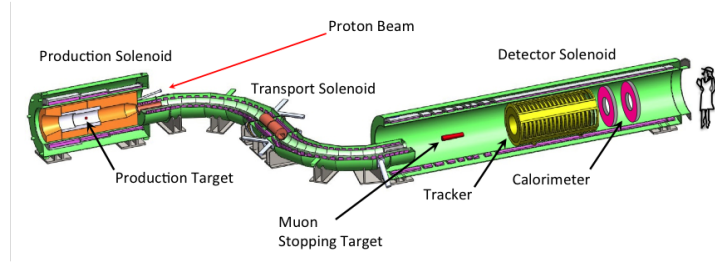


Figure 1.3

The Mu2e experimental apparatus (see Figure 1.3) consists of an integrated array of superconducting toroids, which forms a graded magnetic system that includes the Production Solenoid (PS), the Transport Solenoid (TS) and the Detector Solenoid (DS). (To see all the details reference to [2]). The muon beam is produced using 8 GeV protons from the Fermilab accelerator complex. A bunch of protons with a full width of about 250 ns is steered onto the production target. It consists of a tungsten (W) rod, 160 mm long and with a 6.3 mm diameter, located in the middle of a high-field, graded-field solenoid, the Production Solenoid, which is shown in Figure 1.3.

In the production target, p-W interactions produce pions that are captured into helical trajectories in the field of the solenoid; these pions decay into muons that are also captured by the field of the solenoid. Mu2e collects the backscattered muon beam and transports it into the Transport Solenoid. A thin window in the beginning of TS stops most of the antiproton contamination whilst transmitting almost all of the muons. The TS transmits low momentum negatively charged muons ( $p < 80 MeV/c$ ) into the Detector Solenoid, where they encounter the 34 thin Al foils that comprise the stopping target. The S-shape of TS suppress the line-of-sight neutral particles, while highly energetic negatively charged particles and positively charged particles are suppressed by several absorbers and collimators. In fact, a charged particle beam traversing a curved solenoid will drift perpendicularly to its axis with larger radius for higher momentum and with opposite direction for opposite charge sign. The S-shaped Transport Solenoid consists of a set of superconducting solenoids and toroids forming a magnetic channel that efficiently transmits low energy negatively charged muons from the Production Solenoid to the Detector Solenoid. Negatively charged particles with high energy, positively charged particles and line-of-sight neutral particles are nearly all eliminated by absorbers and collimators before reaching the Detector Solenoid. TS contains three collimators: one at the entrance of TS (TS1), one in the center (TS3), and the last one before entering DS (TS5), (see Figure 1.4).

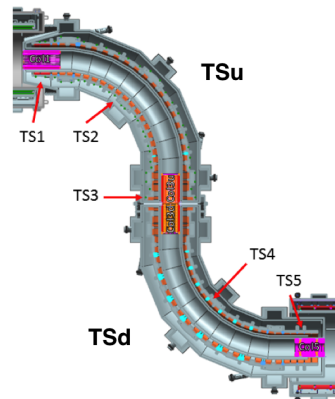


Figure 1.4: The Transport Solenoid

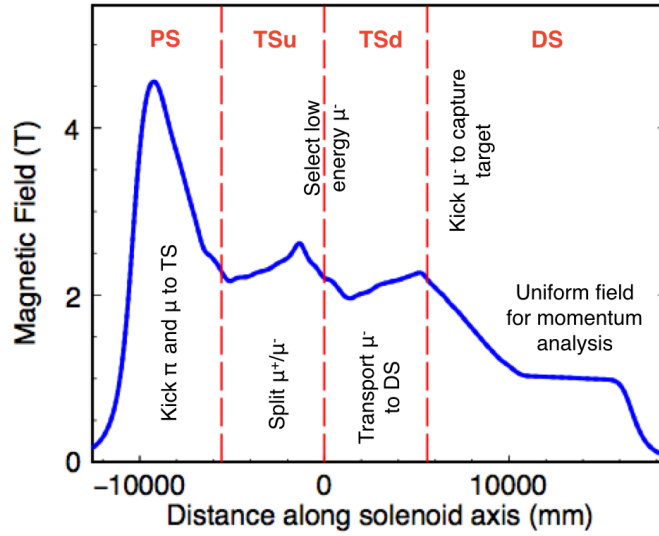


Figure 1.5: Mu2e solenoid system

In Figure 1.5, the shape of the magnetic field is reproduced. The field joint with a complex system of collimators allows particles with right momentum and sign to be selected, as described above. Its values range from a peak of 4.6 T at the upstream end to 1 T at the downstream end.

Downstream of the DS stopping target is a tracking system and downstream of that is an electromagnetic calorimeter. In both of these devices, the inner region, out to a radius of about 38 cm is empty. This allows those muons that do not stop in the stopping target to pass through the detector to the muon beam dump. This also permits the low  $p_T$  subset of the background particles to pass through the detector to the muon beam dump. When a conversion or DIO electron is emitted from the stopping target, it travels in a helical trajectory and, if it has sufficient transverse momentum,  $p_T$ , its trajectory will be measured by the tracker. Only those electrons with  $p_T > 53 \text{ MeV}/c$  will reach the tracker and only those with  $p_T > 90 \text{ MeV}/c$  will intersect enough of the tracker to form a reconstructable track. Because almost all tracks from DIO have  $p_T < m_\mu/2 \simeq 60 \text{ MeV}$ , a large fraction of them (97%) do not reach the tracker. This is the key to making a measurement of  $R_{\mu e}$  with a sensitivity of  $O(10^{-17})$ : the apparatus is only sensitive to the tail of the DIO energy distribution.

### 1.3.1 Mu2e coordinate system

- $(X, Y, Z)$  The Mu2e global cartesian system centered in the middle of TS. In PS and DS the Z coordinate is aligned with the solenoid axis.
- $(u, y, s)$  Coordinate system attached to the Mu2e axis, with the s axis tangent to the symmetry axis (i.e., for PS and DS, parallel to the Z axis in the Mu2e coordinate system), the y axis pointing vertical up (i.e. parallel to the Y axis in the Mu2e coordinates everywhere), and the u axis completing a right-handed cartesian system. In PS and DS, this local system is simply parallel-translated w.r.t. the global Mu2e system in the XZ plane, to have the origin on the Mu2e symmetry axis. In TS, it is both translated and rotated in the XZ plane. In TS3, the positive u axis becomes parallel to the Mu2e positive Z axis and the positive s axis becomes parallel to the Mu2e negative X axis.
- $(s, \phi, r)$  The s is defined as above, r is the coordinate transverse to s and  $\phi$  is the rotation angle (azimuth) around the axis.  $\phi$  is defined so that  $\phi = 0$  corresponds to the +u axis.

## 1.4 Misalignment of the Transport Solenoid

### 1.4.1 Previous study

As explained above, the design of the experiment is based on three superconducting solenoid magnets. The most important uncertainties in the magnetic field of the solenoids can arise from misalignments of the Transport Solenoid, which transfers the beam from the muon production area to the detector area and eliminates beam-originating backgrounds. In previous studies, the field uncertainties induced by possible misalignments and their impact on the physics parameters of the experiment were examined. The work done by Federica Bradascio and Joel Siegel was conducted by using varied field maps, without changing TS geometry (see reference [1]). They examined displacements and rotations about X, Y and Z axis in order to test the sensitivity of the experiment to such misalignments. As these effects occur during the experiment, we cannot directly measure these shifts, but we can understand the effects these shifts will have on the experimental physics parameters. The physics parameters include the muon and pion stopping rates and the scattering of beam electrons off the capture target, which determine the signal, intrinsic background and late-arriving background yields, respectively. Additionally, a possible test of the Transport Solenoid alignment with low momentum electrons is examined, as an alternative to measure its field with conventional probes, which is technically difficult due to mechanical interference.

**Results** The physics parameters were found tolerant within the precision requirements of the experiment for rigid-body type of misalignments, which are the most dangerous, up to a maximum coil displacement of nearly 10 mm, both for muons and pions stopping rates and beam electrons background. With the appropriate choice of low momentum electron detector, the proposed Transport Solenoid test is found sensitive to such misalignments with a high statistical significance. The estimation of beam electrons background gives a much larger value comparing with previous results:  $(2.5 \pm 1.2) \times 10^{-4}$  or  $< 5 \times 10^{-4}$  at 90% C.L. This change is attributed to different methods of simulating electron creation along the beam transport line: in the analysis carrying on by Federica, electrons are created through the entire transport line to the stopping target, whereas in the previous analysis they are created in the upstream half of the transport line. The difference results in a larger number of electrons arriving at the capture target and with a larger spread in the Y dimension, thus scattering more electrons off material, which subsequently hit the tracker. However, this background remains one of the minor backgrounds of the experiment, compared with the dominant DIO background.

### 1.4.2 Purpose of my work

In the present study, I will be focusing on displacements of the central collimator TS3, which plays an important role in the Mu2e system.

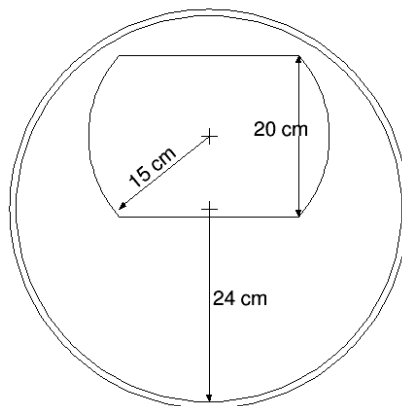


**Figure 1.6:** Cross section of TS3 collimator

As illustrated in Figure 1.6, TS3 is a cylinder with a radius of 24 cm; it is 80 cm long in the

downstream part and 80 cm long in the upstream part and it is made up by copper. It is constructed with an aperture in the upper part to allow negative particles to go through. In fact, negative particles are drifted up by the magnetic field in accordance with their momenta: the higher the momentum the more they are kicked up. The hole is also designed to reduce the background by selecting both the charge of particles and the right momentum range. Therefore, misalignments of the hole could affect charge and momentum range selection. The purpose of my study is to investigate whether the experiment is sensitive to them by examining the effects on the physics parameters. Since this study is a preliminary test, I started with big displacements in the vertical direction by 2 cm up and down and with rotations about  $-X$  and  $+X$  by  $15^\circ$ , as shown in Figure 1.7 and 1.8 for displacements and rotations respectively. Although they are extremely exaggerated misalignments and they should not occur in reality, we need to begin with them in order to maximize what could happen. Later more studies will be done for more realistic displacements by combining the worst cases.

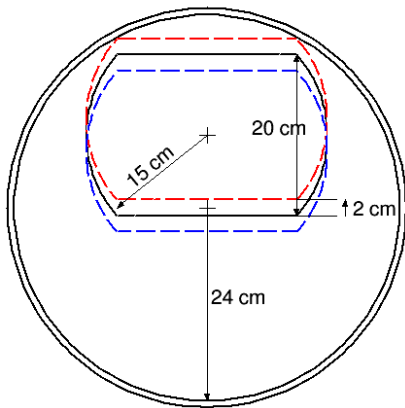


**Figure 1.7:** Displacements up and down by 2 cm

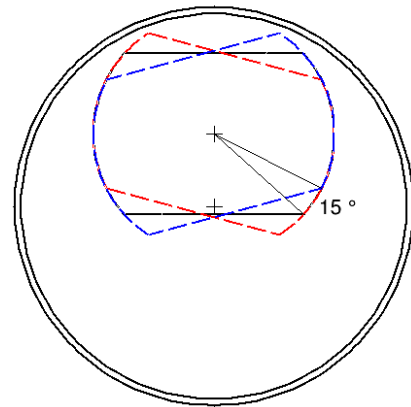


**Figure 1.8:** Rotations by  $15^\circ$  clockwise and counterclockwise

As I described for previous studies, I analyzed the impact of TS3 shifts on the physics parameters, such as the muons and pions stopping rates and the background from beam electrons. Moreover, a test with low momentum electrons was examined in order to trace the field lines by taking advantage of the trajectories of the particles which spiral around them.

The physics simulations are run with GEANT4 ([3]) in the framework of the Mu2e offline software. These simulations make use of only the Mu2e default map, called Mau10. The only changes to the default settings regard the geometry of the system. The simulations are then run on the Fermilab general purpose computer farm called Fermigrid, whereas the results are analyzed locally in ROOT ([4]).

## Chapter 2

# Muons and pions stopping rates

The design of the experiment is based on the minimization or, if possible, elimination of the various backgrounds. For the intrinsic backgrounds, this is achieved by the design of the detector system, whereas for the beam-related backgrounds it is achieved by the design of the beam line and of the data readout timing system, as described previously. The Transport Solenoid plays a key role in the optimal design of the beam line for background reduction, as it filters the particles and transports the beam from the production to the stopping target. The space and time distributions of particles arriving at the stopping target could be affected by TS misalignments. As a result, it changes the yield of muons capture and pions absorption. Therefore, it is essential to determine the tolerance limits for such misalignments on the sensitivity of the experiment.

### 2.1 Stopped particle simulation

I simulated the transport of muons and pions from the production target up to the stopping using single stage simulations with Mu2e Online system. The simulation begins with 8 GeV protons which are modeled as a delta-function in the time domain with an arrival time at the production target of  $t=0$ . The proton-tungsten scattering process, which produces all particles used subsequently in the simulation (scattered protons, knocked-out neutrons, antiprotons, deuterons, pions, kaons, heavier mesons, etc) is a very detailed multi-process cross section model, able to provide the correct particle production fractions (and thus the correct secondary beam admixture) that theory alone cannot. It is developed by the Mu2e group for the purpose of the experiment and it is not in GEANT. The muon and pion simulations were run independently one of each other. I made use of 10 million Protons on Target (POT) for both the simulations. The muons are allowed to decay normally while the pions were forced to remain stable because of their shorter life time of 26 ns, compared with muon lifetime of 2,2  $\mu s$ . If they were allowed to decay, no particles would have reached the stopping target. In order to get a physical meaning to the results, a correction to the data is applied. The final rate is weighted by the decay exponential factor of  $e^{-t/\tau}$  for each pion arrival time  $t$ , where  $\tau$  is the pion lifetime.

### 2.2 Results

I ran simulations for 5 cases:

- the default case, without any shift
- shift up by 2 cm
- shift down by 2 cm
- rotation clockwise (about  $-X$ ) by 15 °
- rotation counterclockwise (about  $+X$ ) by 15 °

The rate of muons and pions is defined as the ratio between the number of particles stopped at stopping target  $Y_{\mu,\pi}$  over the number of protons on target  $Y_{POT}$ :  $R = \frac{Y_{\mu,\pi}}{Y_{POT}}$ . For muons the rate is already computed including the decay law, otherwise the pions rate needs to be weighted.

$$Y_{\pi} = \sum_{i=1}^{N_{\pi}} \exp \frac{-t_i}{\tau} \quad (2.1)$$

For the muon yield,  $Y_{\mu} = N_{\mu}$ , to use a consistent notation.

In order to understand the change if misalignments occur, I calculate the fractional yield difference between the varied case and the default one,  $\alpha$ :

$$\alpha = \frac{Y_{varied} - Y_{default}}{Y_{default}}, \quad (2.2)$$

with the relative error

$$\delta\alpha = \sqrt{\frac{Y_{varied} \cdot (Y_{varied} + Y_{default})}{Y_{default}^3}} \quad (2.3)$$

Below the results are tabulated for all the cases. In Table 2.1 are summarized the muons stopping rates and in Table 2.2 the results for pions. As the purpose of the study is to go on with the work done by F. Bradascio, I touched basis of her work for the default case. For muons, we found consistent results in 1  $\sigma$ ; pion rates cannot be compared though, because a different way to weight the distribution is used.

**Table 2.1:** Muons stopping rates

	$\alpha$ [%]	$Y_{\mu}/Y_{POT}$ [ $10^{-3}$ ]
Federica's default		$1.83 \pm 0.04$
Default		$1.87 \pm 0.01$
Up (2cm)	$-4.55 \pm 1.00$	$1.79 \pm 0.01$
Down (2cm)	$-7.18 \pm 0.98$	$1.74 \pm 0.01$
Right (-X 15°)	$-0.98 \pm 1.03$	$1.85 \pm 0.01$
Left (+X 15°)	$-0.47 \pm 1.03$	$1.86 \pm 0.01$

**Table 2.2:** Pions stopping rates

	$\alpha$ [%]	$Y_{\mu}/Y_{POT}$ [ $10^{-7}$ ]
Default		$6.27 \pm 0.08$
Up (2cm)	$12 \pm 61$	$7.01 \pm 0.09$
Down (2cm)	$-17 \pm 49$	$5.18 \pm 0.07$
Right (-X 15°)	$2 \pm 57$	$6.40 \pm 0.08$
Left (+X 15°)	$4 \pm 58$	$6.53 \pm 0.08$

Looking at the results for muons stopping rates, a decrease of the statistic occurs for the up and down displacements, mainly due to a geometric effect. In fact, when the collimator is displaced, the beam could not overlap the stopping target completely; as a result, some particles are lost. For rotations, consistent results are obtained. As expected, rotations don't affect spiraling particles which can hit the target anyway. Regarding pions, the weighted rates are very low, of the order of  $10^{-7}$ , thus results do not allow significant conclusions. For each case, position and time distributions at the stopping target are examined. Below the plots of the comparison between the default case and the shift up are shown (Figure 2.1 and 2.2). The X and Y profiles are now spread around 0. In particular, the Y distribution reflects the up and down shifts. In fact, the mean value are shifted up and down respectively. However the correlation is not linear. The distribution along Z has a different shape for muons and pions, because of the probability of the processes involved. The probability of a muon to be captured is inversely proportional to its momentum, otherwise pion absorption arises with the momentum. Thus more pions are stopped in the last foils downstream.

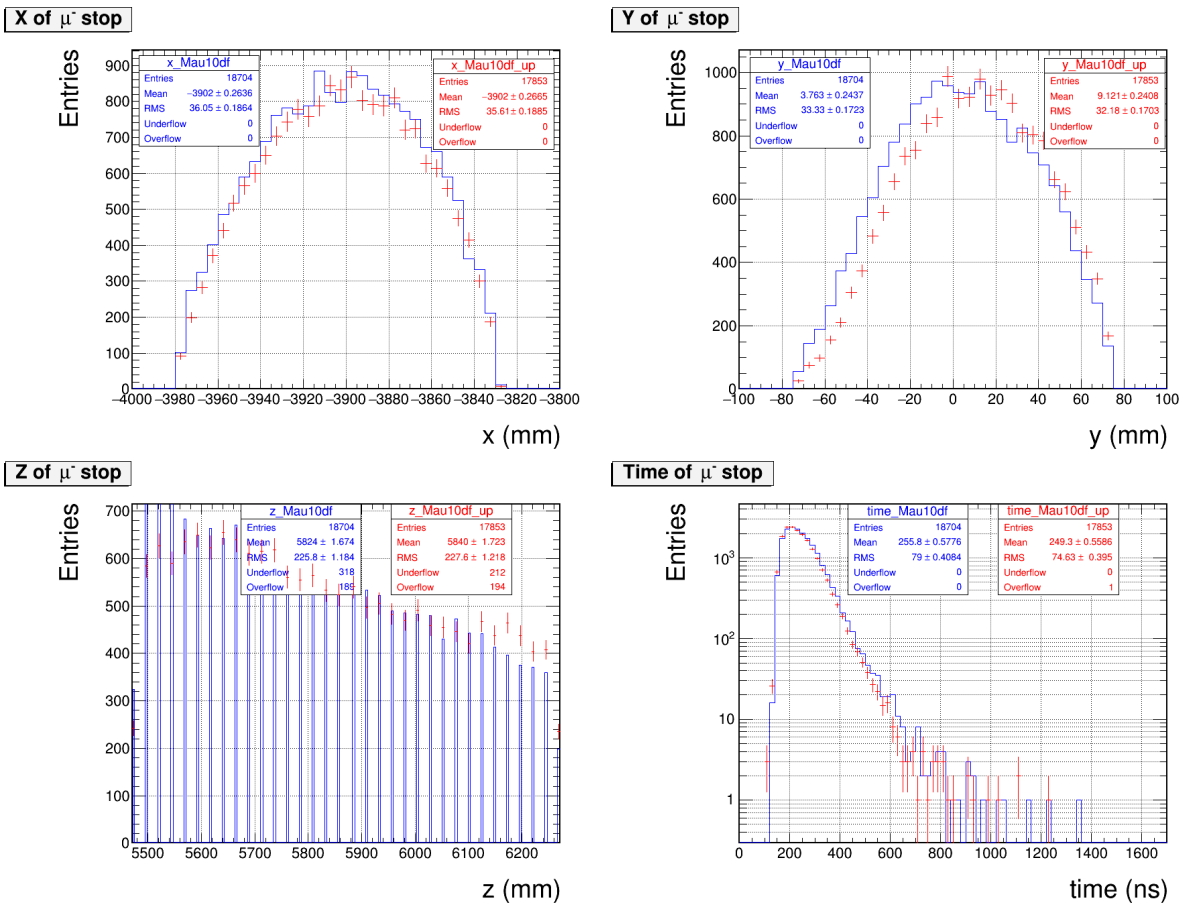


Figure 2.1: X,Y,Z and time distribution for muons for the default case (blue) compared with the shift up.

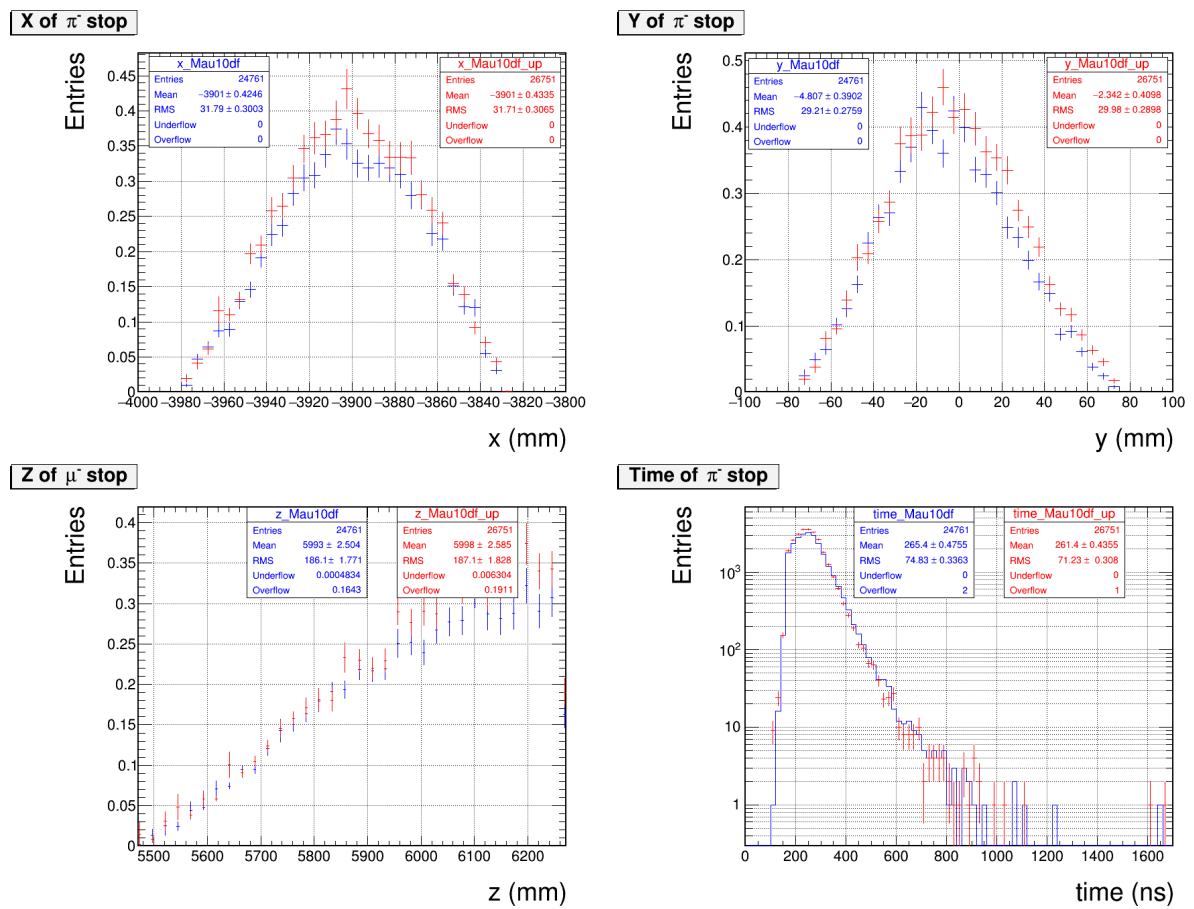


Figure 2.2: X,Y,Z and time distribution for the default case (blue) for pions compared with the shift up.

## Chapter 3

# Beam electrons background

A potential source of background in the Mu2e experiment are high energy electrons that can scatter off of the stopping target and mimic the neutrino less conversion of muons to electrons. The electrons can be produced from the scattering of particles in the Mu2e beam transport line, or from pion decay in the production target. In Mu2e experiment, this background is reduced through three collimators and the magnetic field. These two methods limit the momentum range and the track pitch to the range we would expect the electron conversion to occur at. The collimators in the Transport Solenoid are designed to suppress particles with momenta above 100 MeV/c, while the measured track pitch is required to be between  $0.5 < p_z/p < 0.7$  to reduce background beam electrons from exiting the Transport Solenoid and entering the Detector Solenoid.

### 3.1 Simulation

The simulation has been performed in two stages. First of all, a beam of 8 GeV proton on target interacts in the production target and ends up in the stopping target in DS. At the entrance of the stopping target a virtual detector is located; it is an ideal infinite detector (VD9) which spans all over the transverse plane. The simulation gives as result location, momentum and electrons arrival time, which are saved in a ROOT ntuple. Below the time and momentum distributions are shown as an example.

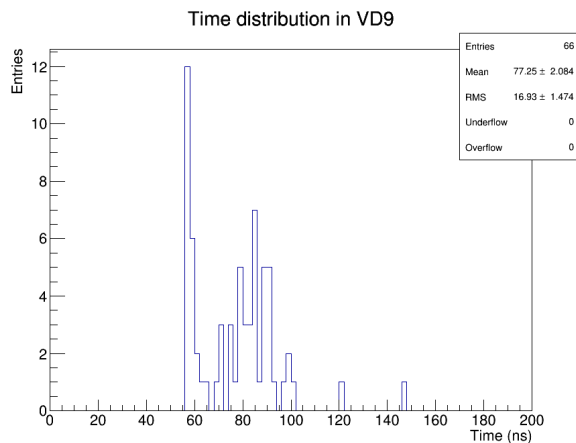


**Figure 3.1:** Time distribution of electrons coming in VD9 for the default case

The plot in Figure 3.1 shows the arrival time of the electrons coming from the single stage simulation at VD9. The pick of arrival times (around 60 ns) cannot be taken as a true value for the extinction electrons background because of the low statistics of the sample comparing with  $10^{20}$  POT of the real experiment. However, the distribution shows an exponential fall-off of the arrival times extending to unlimited times. As a result, some electrons are expected to be in the live window where our signal is. This is a factor to take properly into account in the final estimation algorithm. The simulation gives

also the location of the hits at VD9, as illustrated in Figure 3.2. The electrons hit the virtual detector below the plane because by spiraling around the field lines enter into the DS region in the lower part. To get a clearer explanation, a graph of the motion of low momentum electrons is shown besides the distribution, on the right (Figure 3.3). The electrons travel very closely to the magnetic field lines and so they trace them. Therefore, this picture can be used to see how the field lines are. At the entrance of DS the field lines drop down below the plane, and as explained the electrons do as well.

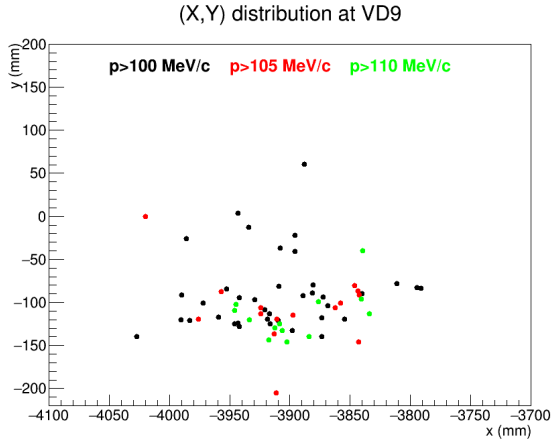


**Figure 3.2:** Scatter plot of X,Y distribution at VD9 for the default case

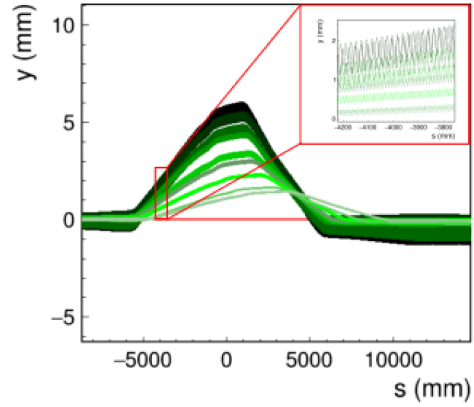


**Figure 3.3:** Trajectory of low momentum electrons with  $0.5 \text{ MeV}/c \leq p \leq 2 \text{ MeV}/c$ , which follow closely the longitudinal field lines.

The number of electrons after the single-stage simulation are of the order of 100 (for the default case just 66) and only few of them will reach the tracker volume. The statistics is orders of magnitude smaller the statistics required to produce a single background event. In order to have an estimation of the background, the statistics needs to be increased. Therefore, in the second stage simulation we made use of a resampling procedure in which each electron is replaced by a cloud of  $10^6$  electrons. The resampled electrons are randomized according to the fit extrapolated from the momentum distribution. The fit function is the following:

$$f(p) = A \cdot e^{-k \cdot (p-p_0)}, \quad \text{where } p_0 = 100 \text{ MeV} \quad (3.1)$$

The position distribution in the x and y axis are randomized according to a gaussian distribution with  $\sigma = 10 \text{ mm}$  and  $\sigma = 10 \text{ ns}$  respectively. In the following Figure 3.4, I show an example of the fit on the momentum distribution on which the resampling is based.

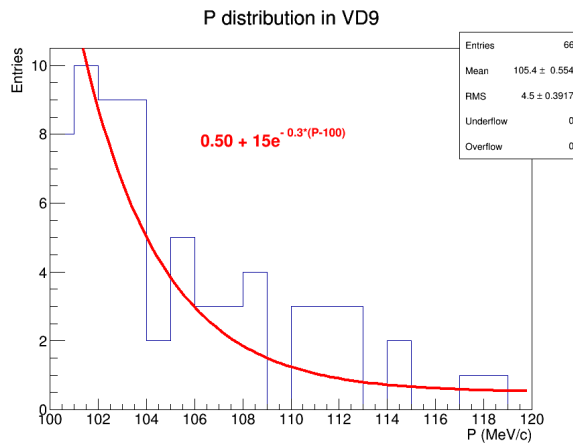


**Figure 3.4:** Momentum distribution at VD9 for the default case. The parameter of the fit are: the constant  $A = 15$  and the slope  $k = 0.3$ .

Resampling over the momenta is a crude approximation, it would be better to resample over the cross section of the Mott scattering. However, in order to get the background estimation, this method is the most efficient in term of computing calculation.

After resampling, the resulting dataset is passed again through the GEANT4 simulation: electrons are sent through the stopping target and the ones which cross the inclusive tracker volume are recorded.

In order to select only electrons which mimic the conversion electrons, a cut on momentum and on the pitch has been applied. Following the selection criteria, the applied cuts are:

- $104 < p < 106$  MeV
- $0.4 < p_z/p < 0.7$

In Figure 3.5, the plots of the electron hits in the tracker volume with different cuts have been compared. The plots 3.5a is filled only by electrons with a momentum above 95 MeV in order to remove low momentum particles. On the right, the electrons in the right momentum range are selected, (Figure 3.5b).

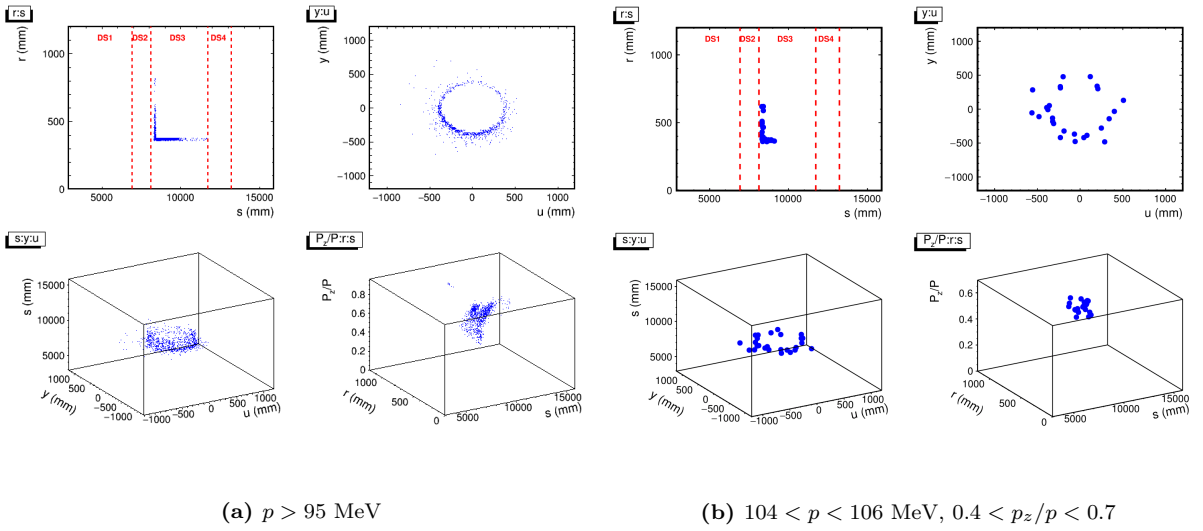


Figure 3.5: Scatter plots of electrons in the tracker volume for the default case.

## 3.2 Results

The purpose of previous studies was to repeat the last estimate for the background which is  $< 5 \cdot 10^{-5}$ . The results were successful and give a value of  $(2.5 \pm 1.2) \cdot 10^{-4}$  for the Mau10 default map. Starting with a beam of  $2.0 \cdot 10^9$  POT, the generate sample of incoming electrons after resampling is  $N_{stat} = 2.0 \times 10^{15}$ . For the default case, only  $N_e = 26$  electrons reach the tracker with the appropriate momenta and pitches. The background has to be rescaled by the total number of protons expected in the experiment  $N = 3 \times 10^{20}$  and multiplied by the extinction factor of  $10^{-10}$ . The last term is the gate life window of the experiment over the total time between two proton bunches. The formula which I used is the following:

$$N_{bkg} \sim \frac{N_e}{N_{stat}} \times 3 \cdot 10^{20} \times 10^{-10} \times 0.5 \quad (3.2)$$

In Table 3.1 are summarized the results of the comparison between the default case and the varied ones. For each case the number of the incoming electrons reaching VD9 and the tracker before and after cuts are reported. An estimation of the background is also computed.

First of all, the results are consistent with the previous study with a difference of less than  $1 \sigma$ ; in this way we got a confirmation of previous results. The only case in which the estimation of the background changes significantly is the displacement up: the background estimate is far away from the default case

**Table 3.1:** Number of electrons at VD9 and at the tracker before and after cuts. In the last column background estimations are compared.

	original $e^-$	$e^-$ @ VD9	$e^-$ @ tracker before cuts	$e^-$ @ tracker after cuts	Background [ $\times 10^{-4}$ ]
Default	$1997 \pm 45$	$66 \pm 8$	6717	26	$(2.0 \pm 0.6)$
up	$2000 \pm 45$	$225 \pm 15$	18531	118	$(9 \pm 1)$
down	$1996 \pm 45$	$22 \pm 5$	4745	40	$(3.0 \pm 0.3)$
Right $15^\circ$	$2000 \pm 45$	$90 \pm 10$	5548	25	$(1.9 \pm 0.7)$
Left $15^\circ$	$1975 \pm 44$	$107 \pm 10$	10067	20	$(1.52 \pm 0.8)$

by  $5\sigma$ . This is expected because electrons drift higher up than muons in the TS3 region, due to a higher velocity distribution corresponding to the same momenta. In equation 3.2 is reported the drift velocity of a relativistic particle in a magnetic field due to the curvature of the solenoid axis with a vector radius  $\vec{R}$ . The drift is perpendicular to the bending plane. The formula depends both on the parallel momentum and the particle velocity. Therefore this explains what I mentioned before.

$$\vec{v}_R = \frac{\vec{p}_{\parallel} \cdot \vec{v}_{\parallel}}{q} \frac{\vec{R} \times \vec{B}}{R^2 B^2} \quad (3.3)$$

where  $E$  e  $B$  are the electric and magnetic field in module.

# Chapter 4

## Beta source test

The idea of the  $\beta$  source test is to use a narrow beam of electrons emitted by a low-energy  $\beta$  source located in PS, and to trace them using a detector located at various positions along the transport line. The principle of the test is that Lorentz forces drive electrons with initial momentum along the field lines to travel through the TS field. Low momentum electrons follow paths very close to the field lines, and thus they can trace the field if they are detected at various positions inside the solenoids.

For the purpose of my work, this test could be of interest because by tracing the locations of the particles it shows what happens before and after the TS3 collimator.

For the test, a source of  $^{90}\text{Sr}/^{90}\text{Y}$  is used, because they have no background and a good momentum range. The spectrum of the total momentum is shown in Figure 4.1 and it derives from the overlap of the two distributions.

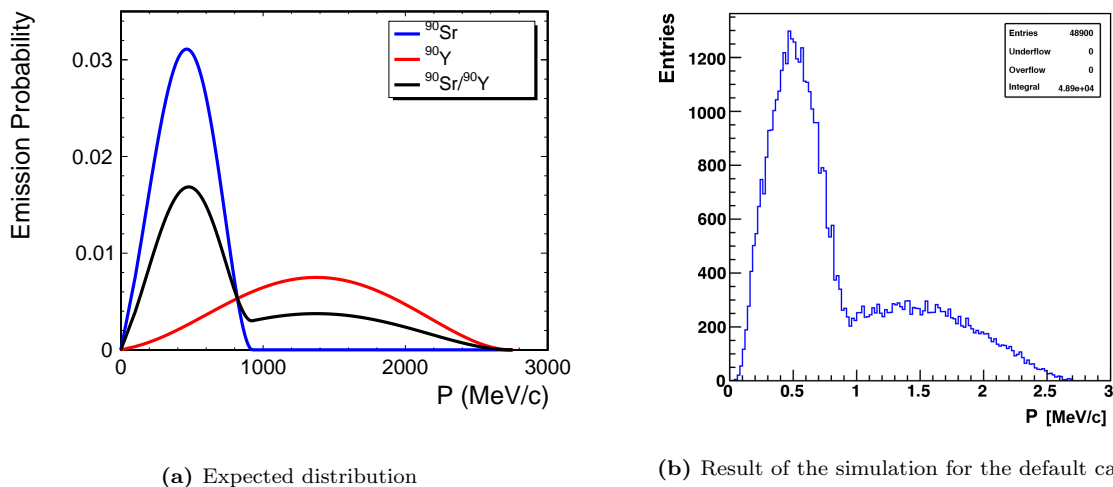


**Figure 4.1:** The momentum distribution of the beta source.

The choice of the detector drives technical requirements for the test, which are high resolution, high efficiency, uniform response and immunity to the magnetic field. The detector could be a scintillator fiber tracker. Its resolution in the (X,Y) plane is of the order of  $\sim 300 \mu\text{m}$  and the minimum momentum threshold for an electron to be detected is  $\sim 200 \text{ keV/c}$ . The pressure is chosen to be low (1 Torr) in order to allow for the electrons to traverse all of TS, otherwise (with higher pressure) they are stopped inside TS because of energy losses in the air.

In Figure 4.2, a schematic picture of Mu2e design is shown with the virtual detector locations along the beam line. I moved parallel both pieces of the TS3 collimator. The upstream piece, called TS3u, is sandwiched by VD3 and VD4 while the downstream piece, called TS3d, is sandwiched by VD5 and VD6. The detectors I am interested in are VD3 and VD4 because I simply test the effects of TS3u. If the collimator is displaced, we expect to see differences in the location and momentum distributions in

VD4 with comparison to VD3.

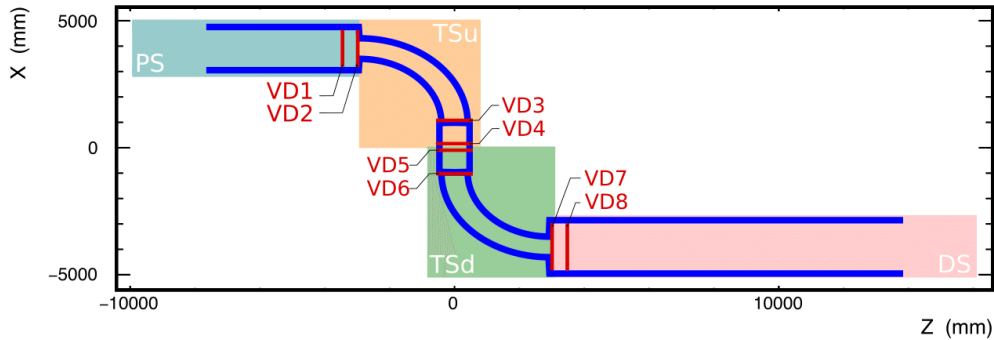


**Figure 4.2:** Virtual detector locations along the beam line. The colored areas show the space covered by the field maps of the four solenoids (PS, TSu, TSd, DS)

## 4.1 Simulations

The test is simulated using the Mu2e Offline Software, in the *art* framework which includes GEANT4. The angles of the electrons are sampled uniformly in the range of  $0^\circ \leq \theta \leq 8^\circ$  and  $0^\circ \leq \phi \leq 360^\circ$  about the Z axis. For each simulation, 27 source locations are used, as shown in Figure 4.3. The source is shifted in the x-y plane relative to the Mu2e coordinate system. The z position of the source is fixed at -6000 mm, before the production target. The y position changes in big steps of 50 mm from 0 to 100 mm above the plane and for small shifts of 5 mm both above and below the plane. The source locations are chosen in order to match with the radius of the TS3 collimator: it allows particles to go through only above the X-Z plane. Moreover, the small shifts help scan the lower edge of the hole inside the collimator in order to see whether cuts of the beam occur.

The electrons hit distribution of the test is represented by scatter plots, as in Figure 4.4. Each plot is the distribution for a different VD. The beam starts in front of the production target in the right location and then it becomes broader and moves in accordance with the field lines.

## 4.2 Results

In my work, I compared the results of the  $\beta$  source test for three different configurations of the TS3 collimator: the default case, the shift up and the shift down by 2 cm.

The mean values are extracted from the 1D plots and the results for all the three cases are compared in Figure 4.5, 4.6, 4.7 for steps of 50 mm, 5 mm above plane and 5 mm below plane. I reported only the results for the virtual detector VD3 and VD4 because, as I said, we are interested in seeing which are the differences caused by TS3 displacements. Looking at the case of 50 mm steps, after the entrance of the TS3 collimator (VD3), I observe that in the last row (for the positions on axis) the mean values are not significant: the up shift is many sigmas away from the default case. This is due to the cut applied by TS3 by moving the collimator up: in such a case a decrease in statistics occurs. In Figure 4.8, scatter plots for one location are shown in order to see the decrease in statistics I mentioned.

This effect is relevant in all the three cases but especially for the small steps below the plane (Figure 4.10), because moving the collimator up, for all the locations the electrons are cut away.

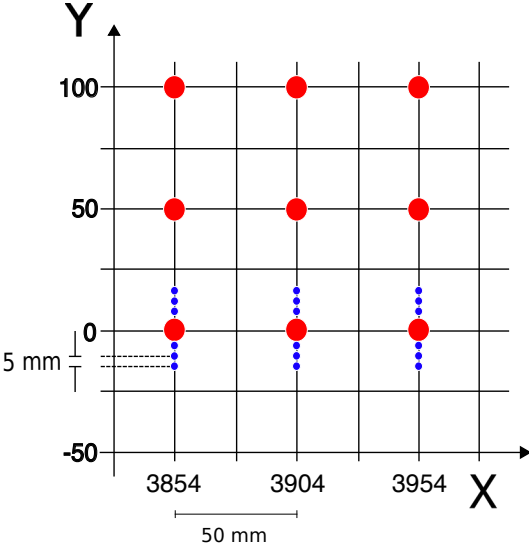


Figure 4.3: Source locations at the production target

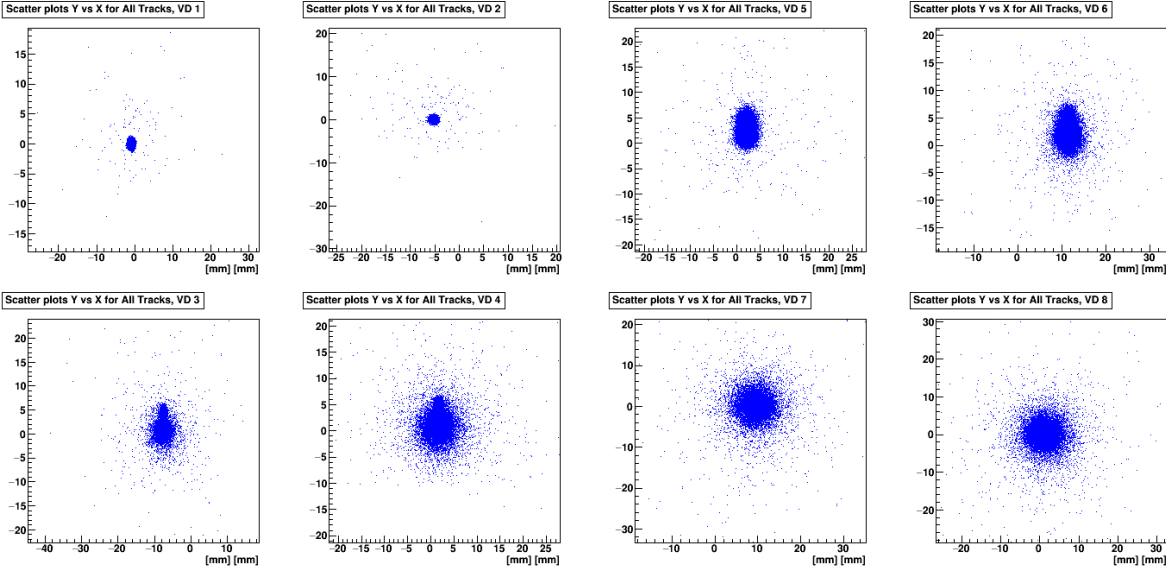


Figure 4.4: Scatter plots in VDs from 1 to 8 for the source location on axis

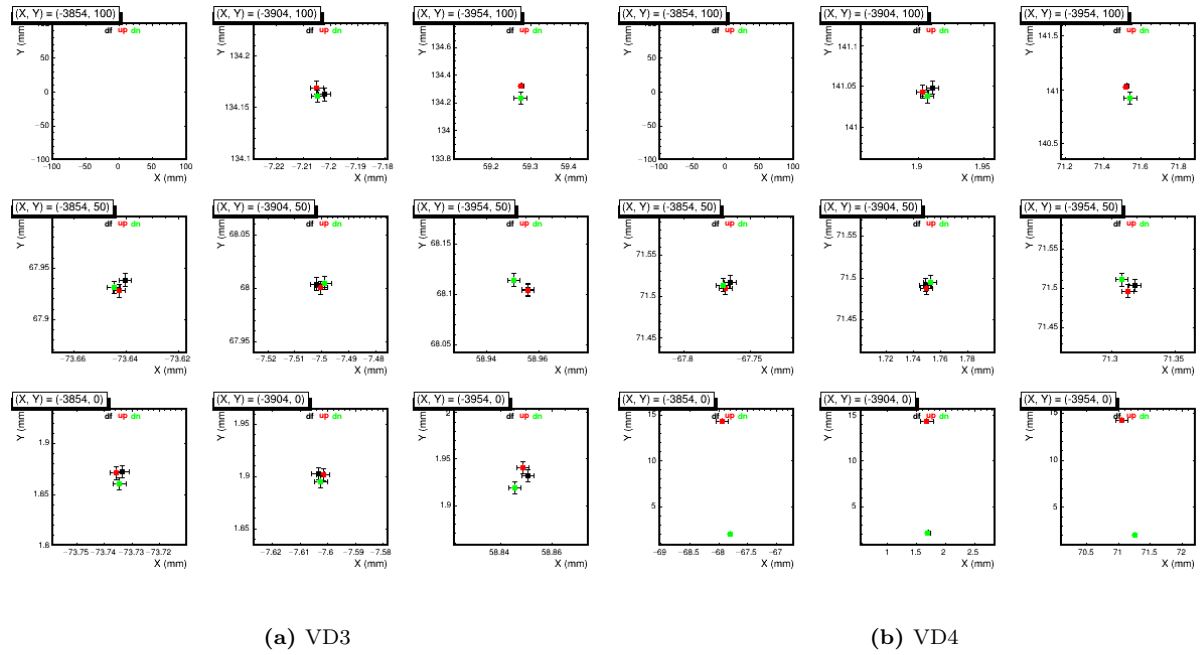


Figure 4.5: Mean values of the default case, the shift up and the shift down for VD3 and VD4, steps of 50 mm

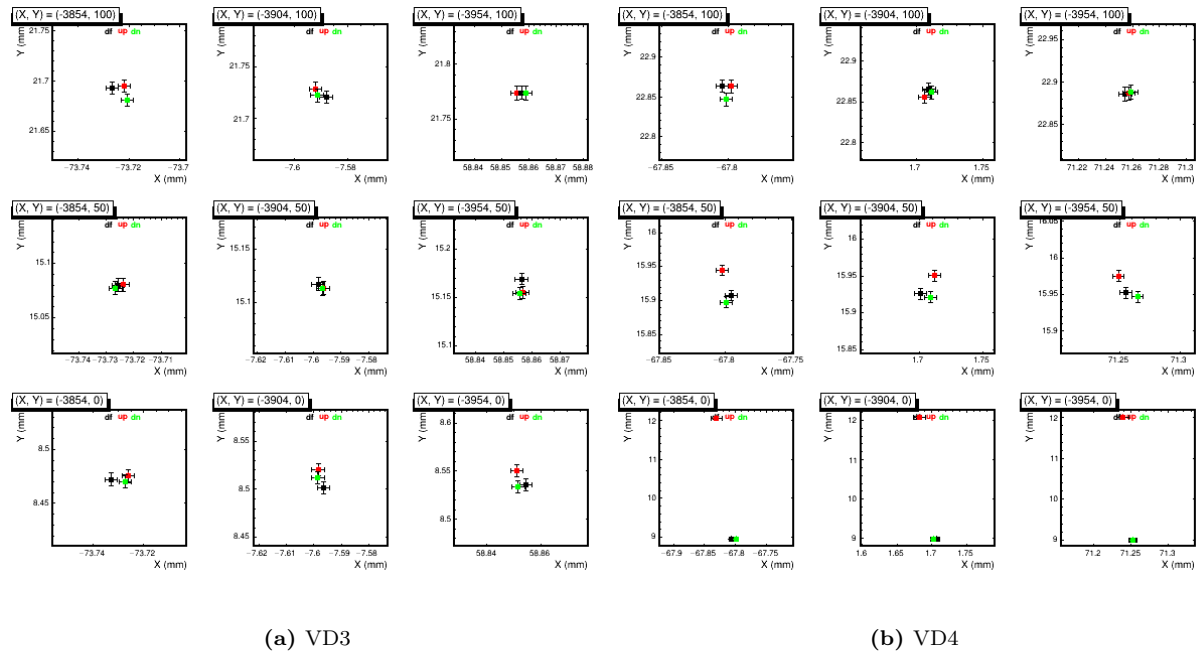


Figure 4.6: Mean values of default case, shift up and shift down for VD3 and VD4, steps of 5 mm above plane

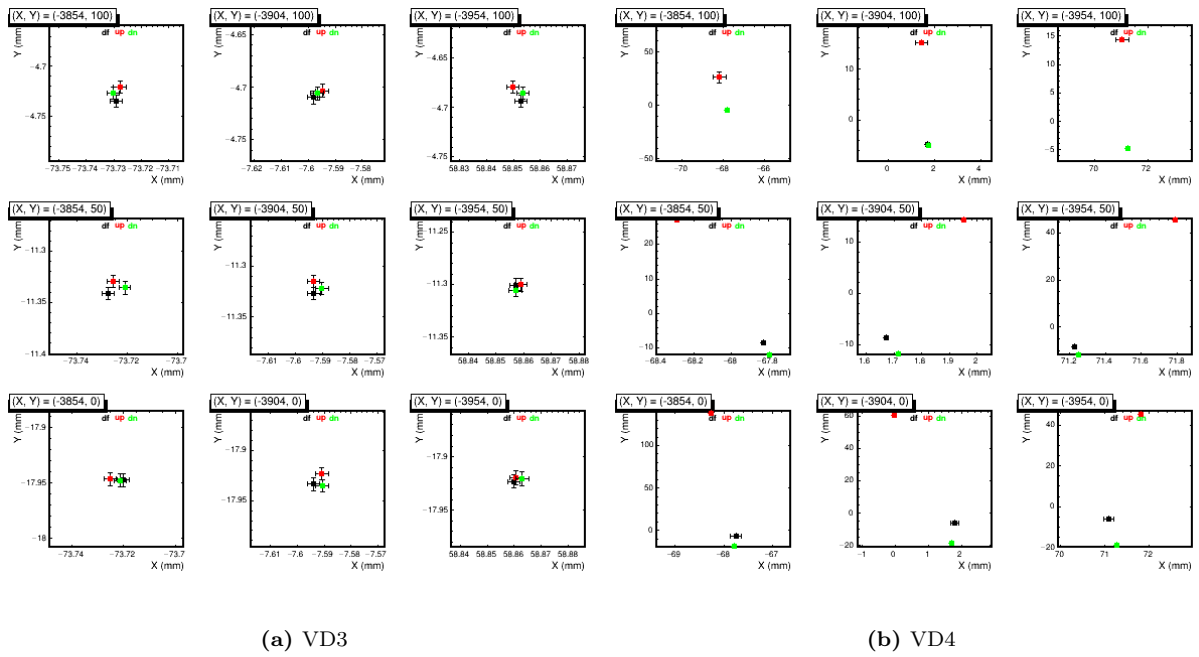


Figure 4.7: Mean values of default case, shift up and shift down for VD3 and VD4, steps of 5 mm below plane

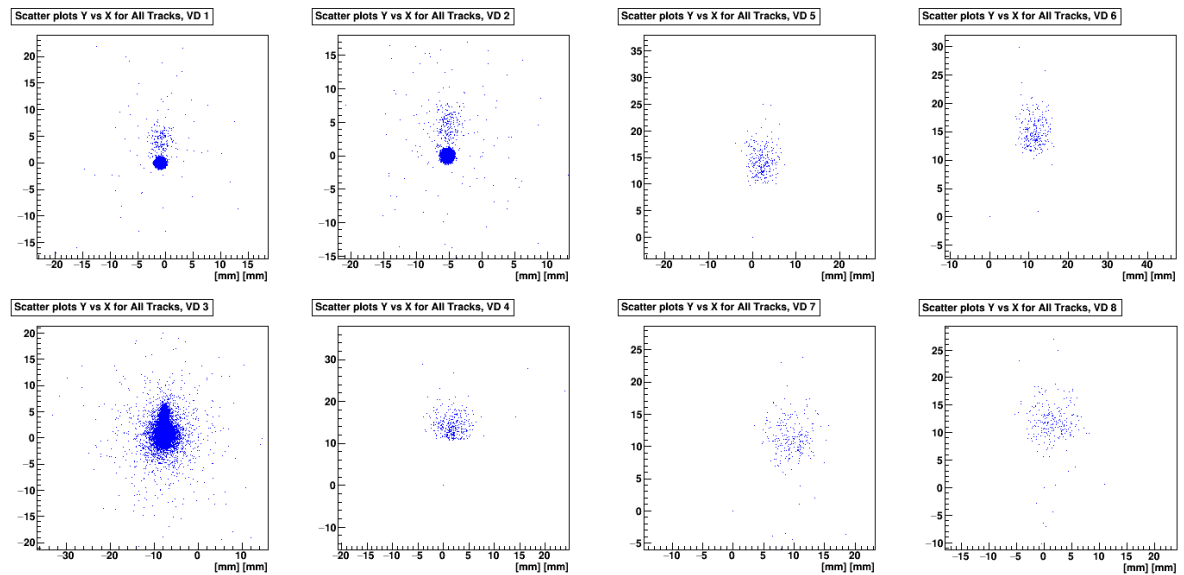


Figure 4.8: Scatter plots for the position on axis (3904, 0), 50 mm steps: 47832 @ VD3, 322 @ VD4

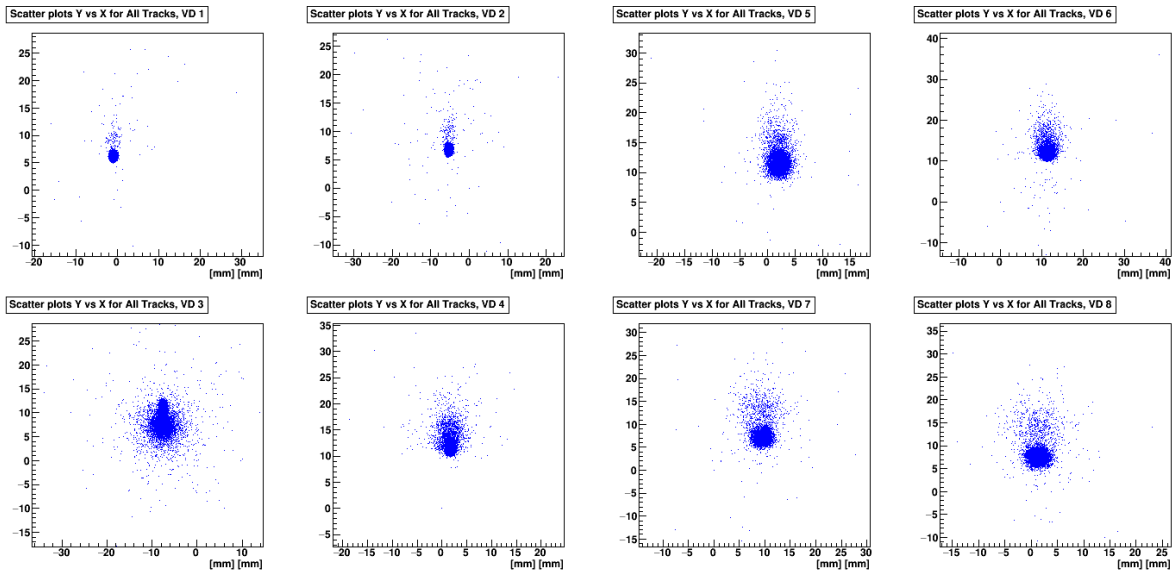


Figure 4.9: Scatter plots for the position on axis (3904, 0), 5 mm steps above plane: 47704 @ VD3, 8045 @ VD4

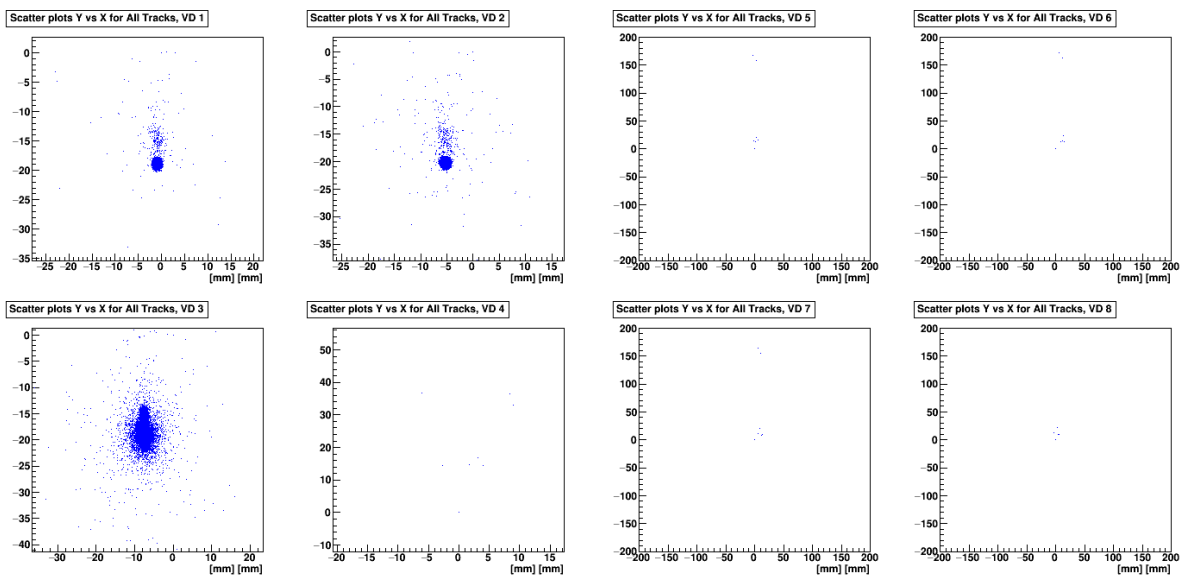


Figure 4.10: Scatter plots for the position on axis (3904, 0), 5 mm steps below plane: 47775 @ VD3, 9 @ VD4

## Chapter 5

# Conclusions

This work aimed to understand the effect of the TS3 collimator misalignments on physics parameters of the experiment. The cases examined are big displacements up and down by 2 cm and rotations of  $15^\circ$  about  $-X$  and  $+X$ . They are all enormously exaggerated misalignments. Although they could not happen in reality, they will be used for future studies to understand what we could expect and leave out some cases, which do not affect physics parameters.

In general, the results showed that only the up and down shifts and only in some cases can impact significantly the physics parameters of the experiment; otherwise rotations do not play an important role.

To discuss the results, I will focus on the main topics I examined one by one: stopping rates, beam electrons background and  $\beta$  source test. Regarding the stopping rates, we carried out that the up and down shifts are important due to a geometric effect. In fact, the beam arriving at the stopping target is significantly displaced by the shifts and it does not overlap completely with the target any longer.

The beam electrons background is sensitive to collimator misalignments; the number of electrons increases as the collimator is shifted upwards. This effect is due to the drift velocity in the magnetic field: the electrons drift higher up than muons in TS3 because of their higher velocity.

Eventually, the  $\beta$  source test is performed. From the simulation we obtained that it is only sensitive to collimator shift up. After the collimator the spots are cut and the corresponding  $\langle Y \rangle$  is shifted up.

The above findings for largely exaggerated misalignments of the TS3 collimator guarantee that the collimator design provides a safe operation point for the experiment.

# Bibliography

- [1] Federica Bradascio Master Thesis, *Studies of the impact of magnetic field uncertainties on physics parameters of the Mu2e experiment*, Mu2e-doc-7808.
- [2] Mu2e Collaboration, *Mu2e Technical Design Report*, (arXiv:1501.05241, 2015).
- [3] Simulation package, *GEANT*, <https://geant4.web.cern.ch/geant4/>.
- [4] Data analysis framework, *ROOT*, CERN, <https://root.cern.ch/>.